Jpn. J. Appl. Phys. Vol. 34 (1995) pp. 161–168
Part 1, No. 1, January 1995

Imaging in an Optical Projection System with a Light Source Composed of Point Sources

Kiichi TAKAMOTO*
NTT LSI Laboratories, 3-1 Morinosato Wakamiya, Atsugi, Kanagawa 243-01, Japan

(Received April 15, 1994; accepted for publication November 19, 1994)

The effects of a points source on imaging characteristics are examined using a one-dimensional model. Intensity distributions for a line-and-space pattern with 5 lines are calculated and the imaging characteristics are evaluated, compared with those obtained using a plane-source system. In a system with a light source composed of 2 point-sources, the focal tolerance determined from linewidth and contrast becomes maximum. Using a light source composed of 3 point-sources, the line-and-space pattern is imaged with precise linewidths while maintaining a focal tolerance slightly larger than that for the plane-source system.

KEYWORDS: optical projection system, imaging, points source, focal tolerance, contrast

1. Introduction

The optical projection system used for microfabrication consists of an incoherent light source, an illumination system and an imaging system. The imaging characteristics are controlled by the coherence factor σ which is defined as the ratio of numerical apertures (NA's) of the illumination system and the imaging system.[1,2] The illumination system NA changes the coherence diameter at the object plane. In this case, the curve representing the relationship between separation and the complex degree of coherence maintains a constant shape. When the plane source is replaced with sources having different forms, the relationship between separation and degree of coherence varies. This is expected to lead to changes in the imaging characteristics.

Improvement of imaging characteristics has been investigated by analyzing the pupil function of the projection lens. Fidelity of intensity distributions in the image field is improved using the apotization method in which the amplitude and phase distribution at the pupil plane in the projection lens is transformed by an appropriate filter.[3,4] It is shown that the Sparrow resolution limit is increased by applying the apodization scheme.[5] The optical modulation function in higher-spatial-frequency domains is increased by placing an annular aperture at the pupil plane. It is shown that the Sparrow resolution is improved using the annular aperture.[6]

In this paper, imaging characteristics of a system having a light source consisting of point sources are analyzed for a one-dimensional model. Intensity distributions for a line-and-space pattern with 5 lines are calculated using the theory of partial coherence.[7] The effects of the number of point sources and the coherence factor on focal tolerance and resolution are examined. The focal tolerances are estimated from intensity distributions in the image field. The imaging characteristics are discussed and compared with the system using a plane source.

*Present address: Research Laboratories, Nippondenso Co., Ltd., 500-1 Minamiyama, Komenoki, Nisshin-shi, Aichi 470-01, Japan.

2. Optical Projection System

An optical projection system composed of an illumination system and a telecentric imaging system is illustrated in Fig. 1. A one-dimensional analysis is carried out for the system under the quasi-monochromatic assumption. Lenses L_1, L_2 and L_3 have the same focal length f. The illumination system composed of a light source and lens L_1 provides Köhler illumination. Light at the source plane is assumed to be incoherent. The imaging system consists of an object plane, lenses L_2 and L_3, a pupil, and an image plane. A reticle, which is an opaque screen with slits, is placed at the object plane. Lenses L_2 and L_3 project the reticle patterns onto the image plane with 1/1 magnification.

The mutual intensity $J_u(u_1, u_2)$ at the object plane is obtained using the Van Cittert-Zernike theorem.[8] $J_u(u_1, u_2)$ for a plane light source is expressed as

$$J_u(u_1, u_2)=\frac{4R_s^2}{(\lambda f)^2}\,\mathrm{sinc}\left[\frac{2\pi}{\lambda f}(u_2-u_1)R_s\right], \tag{1}$$

where λ is the wavelength and R_s is the radius of the source. When the light source is composed of point sources located with equal separation and symmetrical to the optical axis, $J_u(u_1, u_2)$ is expressed as

$$J_u(u_1, u_2)=\begin{cases}\dfrac{4N_p r_s^2}{(\lambda f)^2}\,\mathrm{sinc}\left[\dfrac{2\pi}{\lambda f}(u_2-u_1)r_s\right]\times\displaystyle\sum_{n=1}^{N_p}\exp\left[i\,\dfrac{2\pi}{\lambda f}(u_2-u_1)s_n\right] & \text{for } r_s\neq 0\\[2ex] \dfrac{N_p}{(\lambda f)^2}\displaystyle\sum_{n=1}^{N_p}\exp\left[i\,\dfrac{2\pi}{\lambda f}(u_2-u_1)s_n\right] & \text{for } r_s=0,\end{cases} \tag{2}$$

where r_s is the radius of the point source, s_n is the central coordinate of the n-th point source, and N_p is the number of point sources. A light source composed of multiple point sources is called a points source.

Using mutual intensity relationships for focal plane to focal plane,[7] mutual intensity $J_p(p_1, p_2)$ at the pupil is given by

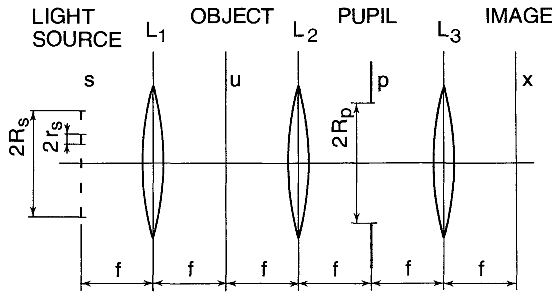

Fig. 1. Configuration of the light source, the illumination system and the imaging system to be analyzed. The light source is composed of point sources.

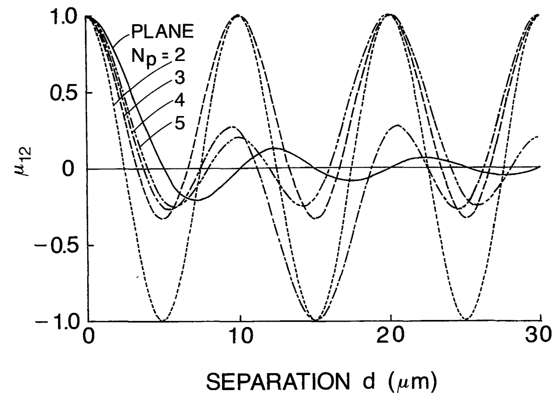

Fig. 2. Relationship between separation d and the complex degree of coherence μ_{12} at the object plane for the plane source and for the points sources. The coherence factor σ for the plane source is 1. The point source radius r_s is 0. The radius R_s of each points source is equal to the radius of the plane source.

$$J_p(p_1, p_2)=\frac{1}{(\lambda f)^2}\iint_{-\infty}^{\infty} J_u(u_1, u_2) \times \exp\left[\mathrm{i}\frac{2\pi}{\lambda f}(p_2u_2-p_1u_1)\right] \mathrm{d}u_1\,\mathrm{d}u_2. \tag{3}$$

When the reticle pattern is projected on the plane located at $(f+\Delta f)$ from lens L_3, intensity $I_x(x;\,\Delta f)$ at defocus Δf is expressed as

$$I_x(x;\,\Delta f)=\frac{1}{(\lambda f)^2}\iint_{-R_p}^{R_p} J_p(p_1, p_2)\exp\left[\mathrm{i}\frac{\pi\Delta f}{\lambda f^2}(p_2^2-p_1^2)\right] \times \exp\left[\mathrm{i}\frac{2\pi}{\lambda f}(p_2-p_1)x\right]\mathrm{d}p_1\,\mathrm{d}p_2, \tag{4}$$

where R_p is the pupil radius. In this paper, intensity distributions are represented using the normalized intensity $I_n(x)$ which is defined as

$$I_n(x)=I_x(x;\,\Delta f)/I(0;\,0). \tag{5}$$

Imaging characteristics are investigated for the system with $\lambda=0.25$ μm, $NA=0.025$ and $f=100$ mm. The Rayleigh resolution limit for a slit is 5 μm. Intensity distributions are calculated for the line-and-space patterns which consist of 5 lines separated by the same distance as the line width. The line widths are chosen to be 3.5, 5, and 8 μm. Although NA is small and the patterns are relatively large for the purpose of reducing the computation time, the imaging characteristics using a points source can be clearly elucidated by comparison with those using a plane source. The computations of the above equations are carried out as rigorously as possible.

3. Complex Degree of Coherence at Object Plane

The complex degree of coherence $\mu_{12}(u_1, u_2)$ at the object plane is given by

$$\mu_{12}(u_1, u_2)=\frac{J_u(u_1, u_2)}{\sqrt{J_u(u_1, u_1)}\sqrt{J_u(u_2, u_2)}}. \tag{6}$$

The complex degree of coherence μ_{12} due to an incoherent light source is a function of separation d, where d is the distance between two u coordinates (u_1, u_2).

Relationships between d and $\mu_{12}(d)$ are shown in Fig. 2 for a plane source and various points sources, where coherent factor σ for the plane source is 1, the diameter of each points source is equal to the diameter of the plane source, and the point source radius is 0. In the region where d is less than 5 μm, points sources produce less coherent light at the object plane than the plane source. As the number of point sources N_p increases, $\mu_{12}(d)$ approaches the curve for the plane source. The function $\mu_{12}(d)$ for the points source, however, is a periodic function of d, so that the functions $\mu_{12}(d)$ for the plane and points sources do not perfectly coincide for any value of N_p. The function $\mu_{12}(d)$ for even-numbered N_p varies between $+1$ and -1, while $\mu_{12}(d)$ for odd-numbered N_p does not reach -1. When N_p is small, the difference in $\mu_{12}(d)$ between the plane and the points sources is very large. It is expected that the system with the points source has imaging characteristics different from those of the plane source system.

The coherence distance d_{co} is defined for the plane source as $d_{co}=\lambda f/(8R_s)$. The complex degree of coherence $\mu_{12}(d)$ for the plane source is equal to 0.9 at $d=d_{co}$. The coherence distance d_{co} plays an important role in imaging. The coherence factor σ for the points source is determined such that the plane and points sources with the same coherence factor σ have the same coherence distance d_{co}.

4. Intensity Distributions

For comparison with intensity distributions due to the points source, intensity distributions due to the plane source are shown in Fig. 3 for (a) $\Delta f=0$ and (b) $\Delta f=200$ μm, where the reticle pattern is a 5 μm line-and-space pattern and σ is 1. Since the complex degree of coherence for incoherent sources does not have an imaginary part, the intensity distributions vary symmetrically with $\pm\Delta f$. In the intensity distributions at $\Delta f=200$ μm, the central, outer, and outermost profiles have almost the same peak and bottom intensities, as well as a similar shape.

The intensity distribution features appear at relatively large Δf. As an example, intensity distributions at $\Delta f=200$ μm for the points source are shown in Fig. 4 for (a) $N_p=2$, (b) $N_p=3$, (c) $N_p=4$ and (d) $N_p=5$,

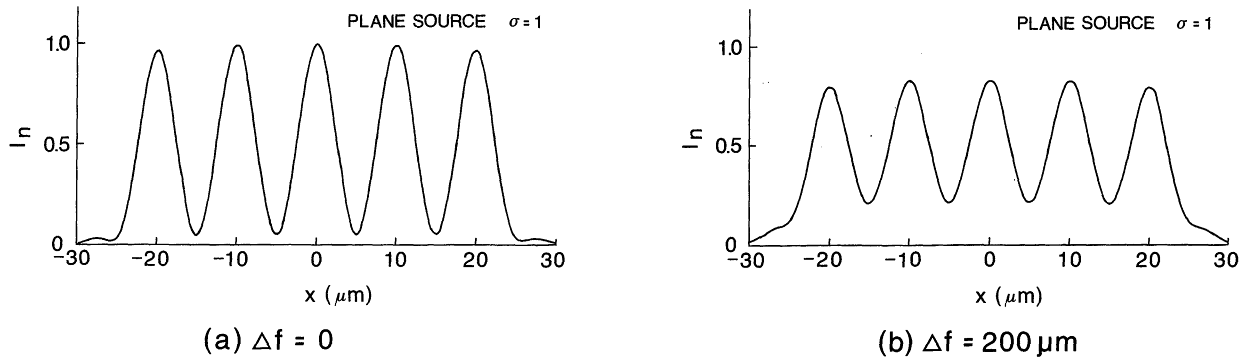

Fig. 3. Intensity distributions due to the plane source, where (a) defocus $\Delta f=0$ and (b) $\Delta f=200$ μm. A 5 μm line-and-space pattern (L&S) with 5 lines is imaged. $\sigma=1$.

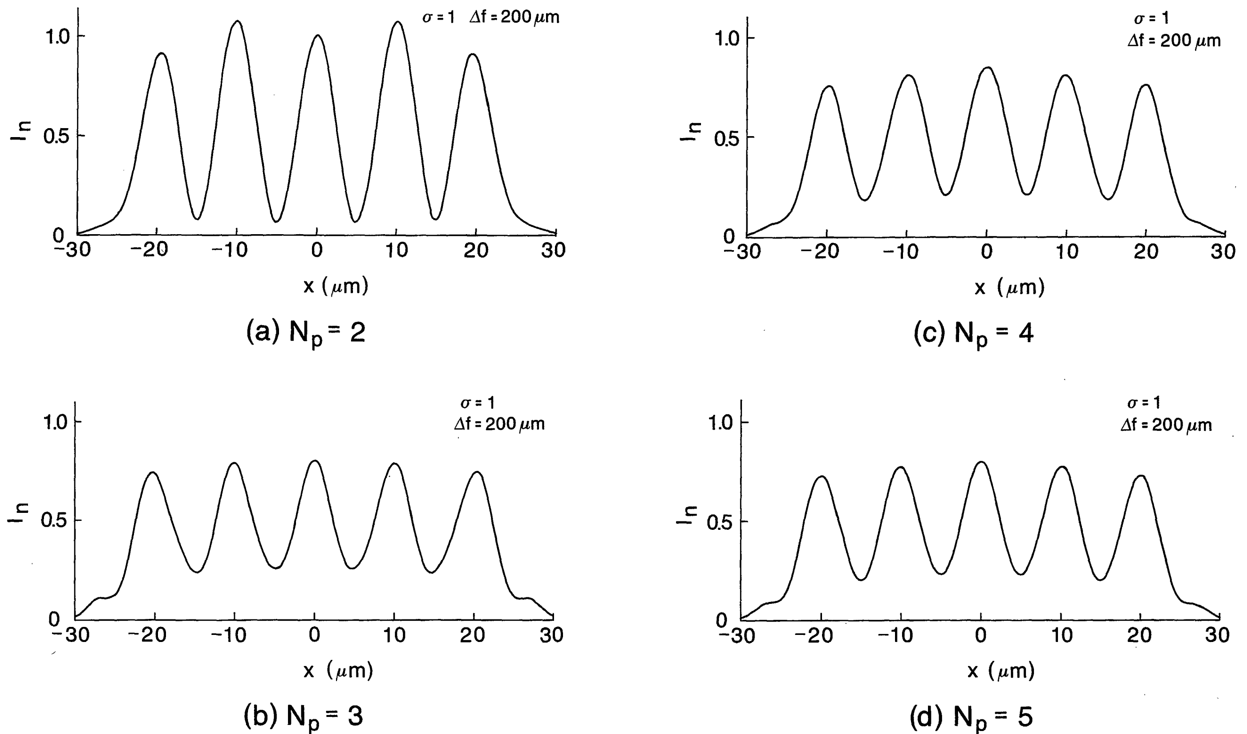

Fig. 4. Intensity distributions at $\Delta f=200$ μm obtained using the points sources with (a) $N_p=2$, (b) $N_p=3$, (c) $N_p=4$, and (d) $N_p=5$. N_p is the number of point sources. $r_s=0$. $\sigma=1$.

where the reticle pattern is a 5 μm line-and-space pattern and $\sigma=1$. When $N_p=2$, the contrast is very high and the peak intensities of profiles are greater than 0.9. The peak intensities for the outer and outermost profiles are not located at $x=10$ μm or 20 μm, respectively. In the distribution for $N_p=3$, the bottom intensities between profiles become higher and the profiles have lower contrast than the profiles for $N_p=2$. When $N_p=4$, the difference in peak intensity between the central and the outermost profiles is relatively large. Light intensity has a tendency to be concentrated in the central profile. The peaks of the outer and outermost profiles for $N_p=5$ lie at $x=10$ μm and 20 μm, respectively. The system with a points source produces intensity distributions having notable features.

5. Focal Tolerance

The intensity distribution at $\Delta f=0$ for a line-and-space pattern with 5 lines is illustrated in Fig. 5. Profiles P_0, P_1, and P_2 indicate central, outer, and outermost profiles, respectively. Definitions of linewidth and location of each profile are also shown in Fig. 5. The threshold intensity I_{th} is defined as the intensity which gives the designed line width to the central profile P_0 in the intensity distribution at $\Delta f=0$. For intensity distributions at various Δf, the linewidth for each profile is evaluated from two x coordinates where I_{th} coincides with the profile curves. The location of each profile is obtained by averaging the two x coordinates. Linewidth deviation ΔW is defined as $\Delta W=W_c-W_d$, where W_c is the linewidth obtained from the calculated intensity distribution and W_d is the designed line

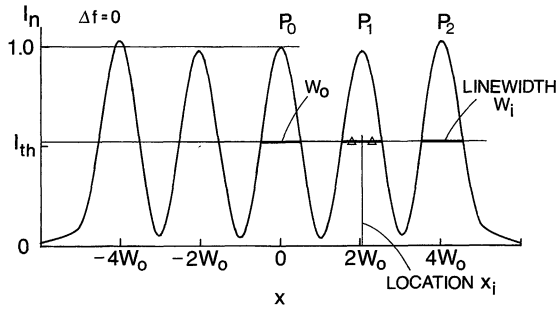

Fig. 5. Illustration of intensity distribution at $\Delta f=0$ for a line-and-space pattern with 5 lines. W_o is the linewidth at the object plane.

width. Location shift Δx of profiles is defined as $\Delta x=x_c-x_d$, where x_c is the location of the calculated profile and x_d the designed location. Profile contrast C is defined as

$$C=(I_{\max}-I_{\min})/(I_{\max}+I_{\min}), \tag{7}$$

where $I_{\max}$ is the peak intensity of the profile and $I_{\min}$ is the minimum intensity around the profile. $I_{\min}$ for P_2 is taken to be the minimum intensity between P_1 and P_2.

Conventionally, focal tolerance is evaluated by $\pm 0.5\lambda/NA^2$. This focal tolerance becomes ± 200 μm for $\lambda=0.25$ μm and $NA=0.025$. In this paper, focal tolerances FT_w for linewidth and FT_c for contrast are defined individually. When Δf is between $\pm FT_w$, the linewidth variation is within ± 0.5 μm. When Δf is between $\pm FT_c$, the contrast is higher than 0.5.

5.1 *Plane source*

The effect of Δf on ΔW and C at $\sigma=0.75$ is shown in Fig. 6 for (a) 8 μm, (b) 5 μm, and (c) 3.5 μm line-and-space patterns. In Fig. 6(a), linewidths increase with increasing Δf. The difference in linewidth among P_0, P_1, and P_2 is relatively small. The profiles have almost the same contrast. In Fig. 6(b), linewidths of P_0 and P_1 vary negligibly with Δf, while the linewidth of P_2 decreases with increasing Δf. The contrast is lower than for the 8 μm line-and-space pattern. In Fig. 6(c), the contrast is less than 0.5. The relationship between Δf and Δx for P_1 and P_2 is shown in Fig. 7. In the case of P_1, Δx is smaller for line-and-space patterns with narrower line widths. However, Δx of P_2 is larger for the 5 μm than for the 3.5 μm line-and-space patterns when Δf is less than 110 μm.

The dependences of FT_w and FT_c on σ for the 5 μm line-and-space pattern are shown in Fig. 8. Also shown are P_1 and P_2 linewidths at $\Delta f=0$. Variation of the P_1 linewidth with σ is small. The P_2 linewidth decreases as σ increases from 0 to 1. P_2 has a larger linewidth than P_1 for $\sigma\leq 0.5$. When a line-and-space pattern at the object plane is illuminated by completely coherent light, the light intensity at the image is redistributed so as to accumulate more light intensity in the outer lines than in the inner lines. As the degree of coherence at the object plane degrades from complete coherence, the intensity redistribution effect becomes weaker. Differences in linewidth among the profiles are smallest at $\sigma=0.5$. The focal tolerances become lower for coherent ($\sigma=0$) and incoherent ($\sigma=\infty$) illuminations than for partially coherent illumination. A coherence factor σ optimized for the focal tolerances exists. The optimized σ is 0.5 for the linewidth and 0.75 for the contrast. Taking the linewidth and contrast focal tolerances into account, $\sigma=0.75$ is more reasonable for patterning.

The relationship between Δf and Δx of P_1 and P_2 for a 5 μm line-and-space pattern is shown in Fig. 9. P_1 and P_2 move from the designed locations. The location shift Δx is dependent on σ. For $\sigma=0.25$, Δx of P_2 is as large as 0.3 μm at $\Delta f\leq 50$ μm. For $\sigma=0.5$, Δx of P_1 and P_2 is less than 0.05 μm at $\Delta f\leq 150$ μm.

5.2 *Points source*

Light cannot be focused to a point source with $r_s=0$. On the right side of eq. (2), the sinc function becomes

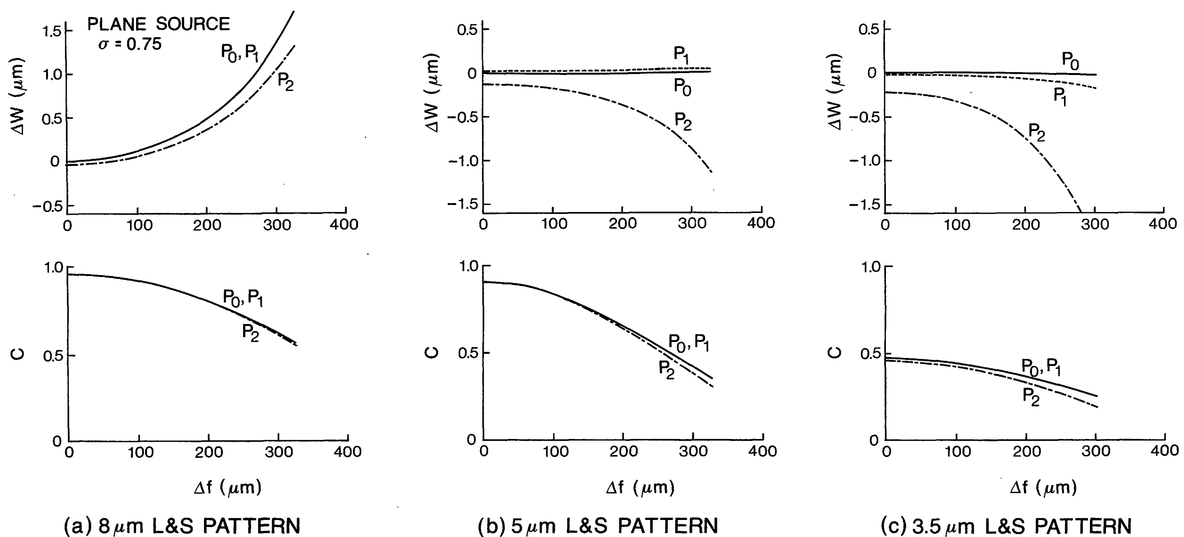

Fig. 6. Effect of Δf on linewidth deviation ΔW and contrast C for the system with the plane source. Imaged patterns are (a) 8 μm, (b) 5 μm, and (c) 3.5 μm line-and-space patterns. P_0, P_1, and P_2 denote central, outer, and outermost profiles, as shown in Fig. 5. $\sigma=0.75$.

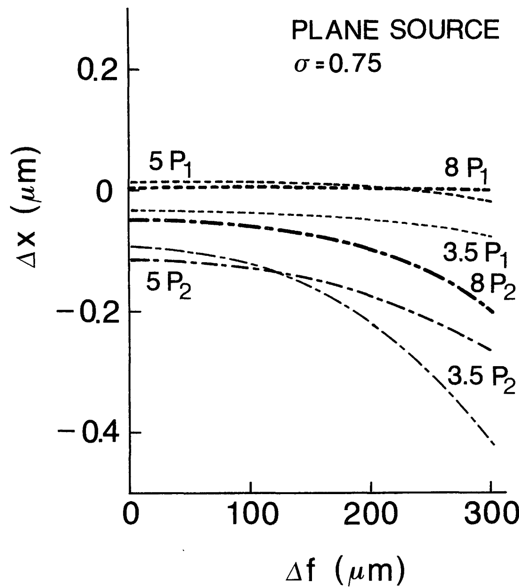

Fig. 7. Relationship between Δf and location shift Δx for P_1 and P_2. The system has a plane source. The line width of the line-and-space pattern is denoted by W of $W\,P_n$ $(n=1, 2)$ in the figure. $\sigma=0.75$.

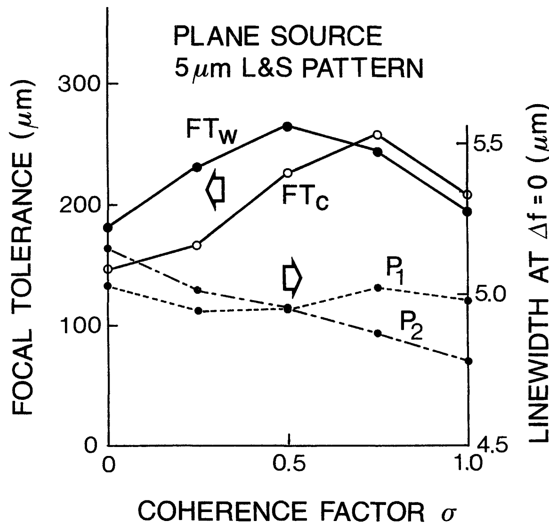

Fig. 8. Dependence of focal tolerance on σ for the system with the plane source. Linewidths of P_1 and P_2 at $\Delta f=0$ are also shown. The imaged pattern is a 5 μm line-and-space pattern. As for the focal tolerance FT_w for line width, the line width variation is less than ± 0.5 μm at Δf between $\pm FT_w$. As for the focal tolerance FT_c for contrast, the contrast is above 0.5 at Δf between $\pm FT_c$.

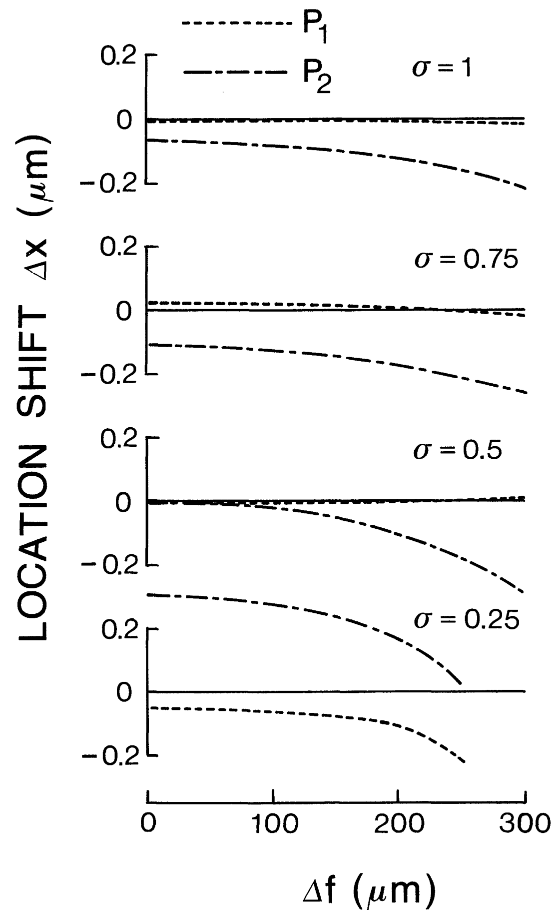

Fig. 9. Relationship between Δf and Δx for P_1 and P_2 for (a) $\sigma=1.0$, (b) $\sigma=0.75$, (c) $\sigma=0.5$ and (d) $\sigma=0.25$. The imaged pattern is a 5 μm line-and-space pattern.

nearly equal to 1 for r_s of less than 10 μm in the range of parameters used in this analysis. Therefore, the following calculations are performed for the points source with $r_s=0$.

The effects of N_p on the focal tolerances and linewidths at $\Delta f=0$ are shown in Fig. 10 for (a) $\sigma=1$, (b) $\sigma=0.75$, and (c) $\sigma=0.5$, where the object is a 5 μm line-and-space pattern.

In Fig. 10(a), imaging characteristics such as focal tolerance and linewidth almost coincide for the 12-points source and plane source systems. P_2 has a narrower linewidth than P_0 and P_1. FT_w is strongly dependent on P_2 linewidth at $\Delta f=0$. When $N_p=4$, the P_2 linewidth at $\Delta f=0$ is narrower than 4.5 μm, so that FT_w does not exist. Compared with the plane source system, FT_w is deeper for N_p execpt for $N_p=4$–6 and 8. FT_c is deeper for $N_p=2$ and 4 than for the plane source. The points source with $N_p=3$ produces the maximum FT_w, but FT_c is narrowest. In particular, the tolerance for $N_p=2$ is much deeper than for the other cases. The complex degree of coherence due to the 2-points source becomes -1 at separation $d=8.7$ μm. The light fields separated by 8.7 μm oscillate in opposite directions. It was shown that the resolution was improved using a phase-shift mask.[9] It is expected that the 2-points source will produce a similar effect as the phase-shift mask.

In Fig. 10(b), FT_w and FT_c are deeper except for FT_w at $N_p=2$ than in Fig. 10(a). When $N_p=3$ and 5, linewidths of P_1 and P_2 are larger than that of P_0. One method of preventing the outermost lines from becoming narrower than the inner lines is to employ the plane source illumination with σ less than 0.3. This method, however, induces narrower focal tolerances as shown in Fig. 8. In the case of $N_p=3$ with $\sigma=0.75$, the degree of coherence becomes 1 when the separation is a multiple of 19 μm. The degree of coherence between light il-

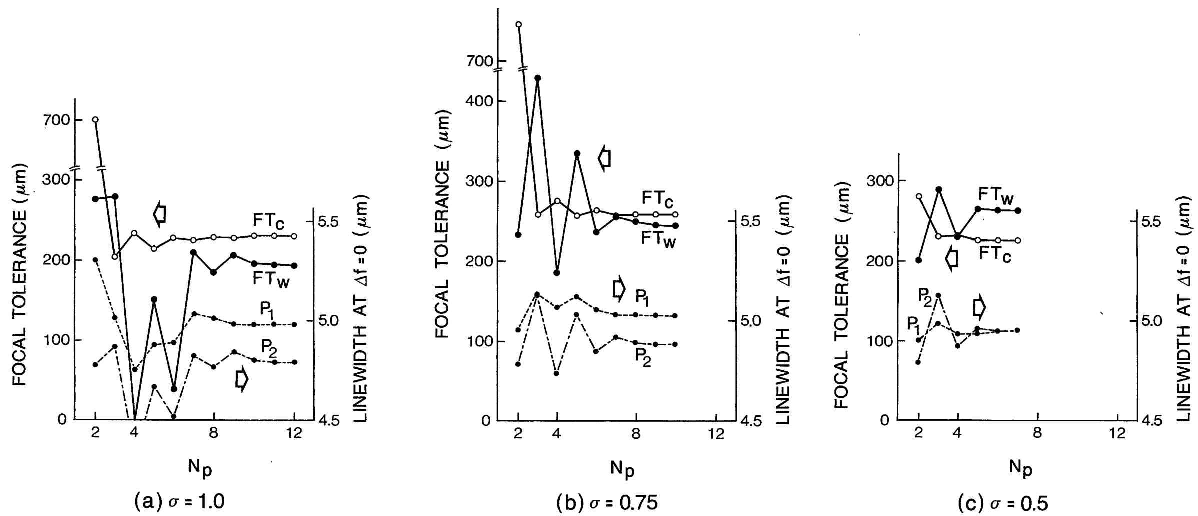

Fig. 10. Effects of N_p on FT_w and FT_c for (a) $\sigma=1.0$, (b) $\sigma=0.75$, and (c) $\sigma=0.5$. Linewidths of P_1 and P_2 at $\Delta f=0$ are also shown. The imaged pattern is a 5 μm line-and-space pattern. $r_s=0$.

luminating line patterns at the object plane is relatively high, thus this illumination produces almost the same effect as plane source illumination with a low coherence factor. The imaging characteristics for N_p larger than 9 almost coincide with those due to the plane source.

In Fig. 10(c), the effects of the points source are less conspicuous compared with Figs. 10(a) and 10(b). This is because $\mu_{12}(d)$ values for the points sources and the plane source are almost coincident in the area of a line-and-space pattern at the object plane. The points sources with N_p greater than 6 produce almost the same imaging characteristics as the plane source with $\sigma=0.5$.

In the case of $N_p=2$ with $\sigma=1$, FT_w and FT_c are very large compared with the other cases. For the 2-points source system with $\sigma=1.25$, intensity distributions for a 5 μm line-and-space pattern are calculated, but the P_2 linewidth at $\Delta f=0$ is smaller than 4.5 μm. The system having a 3-points source with $\sigma=0.75$ produces intensity distributions without narrowing of the outermost profiles while maintaining relatively large focal tolerances. Therefore, we will examine the image characteristics due to the points sources with $N_p=2$ and 3 in more detail.

5.3 *Two-points source system with* $\sigma=1$

Intensity distribution at the pupil of the imaging system is shown in Fig. 11, where a 5 μm line-and-space pattern is placed at the object plane. A major portion of light passes through the region around $p=1.43$ mm. This shows that the system with a 2-points source exerts an effect on imaging which is similar to that of the plane source system having an annular aperture at the pupil of the projection lens. The difference between the two systems is that the optical transfer function for the 2-points source system does not have the spatial frequency domain where some frequencies completely disappear.

The effects of the radius r_s of a point source on FT_w and FT_c^* are shown in Fig. 12, where the object is a 5

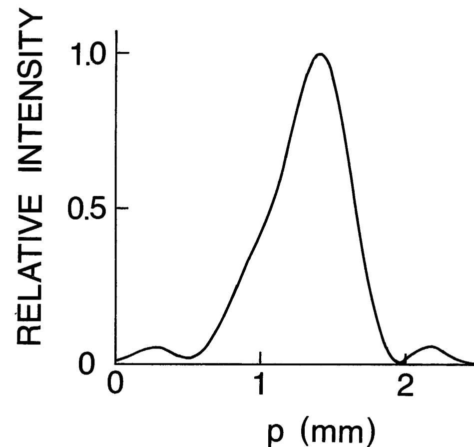

Fig. 11. Intensity distribution at the pupil plane in the projection lens system, where $N_p=2$ and $r_s=0$. The pattern at the object is a 5 μm line-and-space pattern.

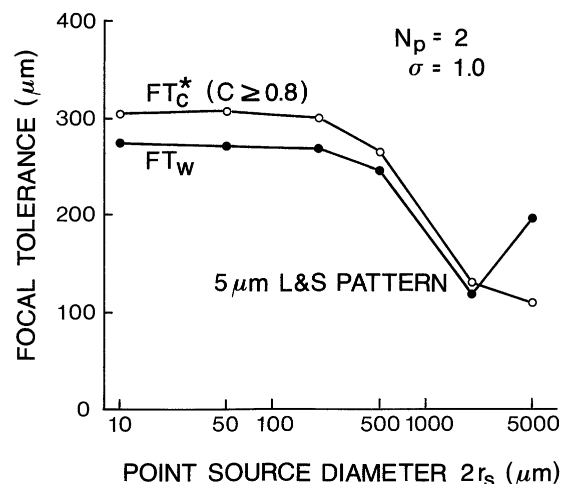

Fig. 12. Effects of $2r_s$ on FT_w and FT_c^*. The system has a 2-points source with $\sigma=1$. FT_c^* is evaluated from Δf where the contrast C is larger than 0.8. The imaged pattern is a 5 μm line-and-space pattern.

μm line-and-space pattern. In the case of $N_p=2$ and $\sigma=1$, contrast is very high, so that FT_c^* is evaluated for a contrast of more than 0.8. In the region where r_s is less than 100 μm, FT_w and FT_c^* decrease slightly with increasing r_s. When $r_s=1$ mm, FT_w becomes smaller than for $r_s=2.5$ mm, equivalent to the plane source.

Dependences of line width and contrast on Δf are shown in Fig. 13 for (a) 8 μm, (b) 5 μm, and (c) 3.5 μm line-and-space patterns. Compared with Fig. 6 for the plane source, linewidth and contrast vary slowly with increasing Δf. For example, the contrast at $\Delta f=0$ for the 8 μm line-and-space pattern is lower in Fig. 13(a) than in Fig. 6(a), but Δf where the contrast decreases to 0.8 is deeper. The improvement in contrast is more marked for finer line-and-space patterns. Intensity distributions for a 3.5 μm line-and-space pattern have a contrast of more than 0.8 at $\Delta f \leq 125$ μm. Generally, intensity distributions at Δf beyond a certain value are deformed so that 5 line profiles cannot be resolved. When $N_p=2$, the P_2 linewidth becomes thinner for larger Δf, but 5 line profiles are clearly separated because of the high contrast. It is thought that intensity distributions with high contrast and high resolution are attained through a combination of two effects that are similar to the annular aperture and the phase-shift mask.

The relationship between Δf and Δx is shown in Fig. 14 for 8, 5, and 3.5 μm line-and-space patterns. When a 5 μm line-and-space pattern is imaged, Δx at $\Delta f=0$ is large, but P_1 and P_2 have a tendency to approach the designed locations as Δf is increased.

5.4 *Three-points source system with $\sigma=0.75$*

The dependences of line width and contrast on Δf are shown in Fig. 15 for (a) 8 μm, (b) 5 μm, and (c) 3.5 μm line-and-space patterns. Compared with Figs. 6 and 13, the linewidths vary slowly with Δf, and each profile shows a more precise linewidth. The contrast for 8 and 5 μm line-and-space patterns is slightly lower than that for the plane source with $\sigma=0.75$. In Fig. 15(c) for a 3.5 μm line-and-space pattern, the contrast is higher than in Fig. 6(c) for the plane source.

The relationship between Δf and Δx is shown in Fig. 16. The location shifts Δx for a 5 μm line-and-space pattern are larger than those for 8 μm and 3.5 μm line-and-space patterns. Compared with the plane source and the 2-points source, the variation in profile location with Δf is pronounced.

6. Conclusions

An optical projection system with a light source composed of point sources is investigated using a one-dimensional model. Intensity distributions are calculated for a line-and-space pattern with 5 lines. Imaging characteristics of the points source become almost the same as that of the plane source when the number of

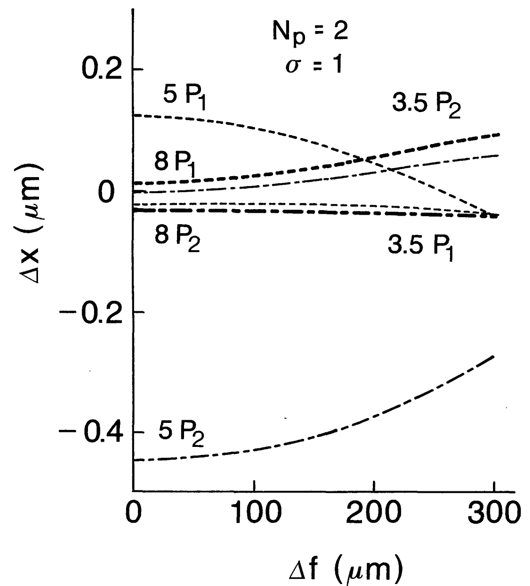

Fig. 14. Relationship between Δf and Δx for P_1 and P_2. The system has a 2-points source with $r_s=0$ and $\sigma=1$. Imaged patterns are 8 μm, 5 μm, and 3.5 μm line-and-space patterns.

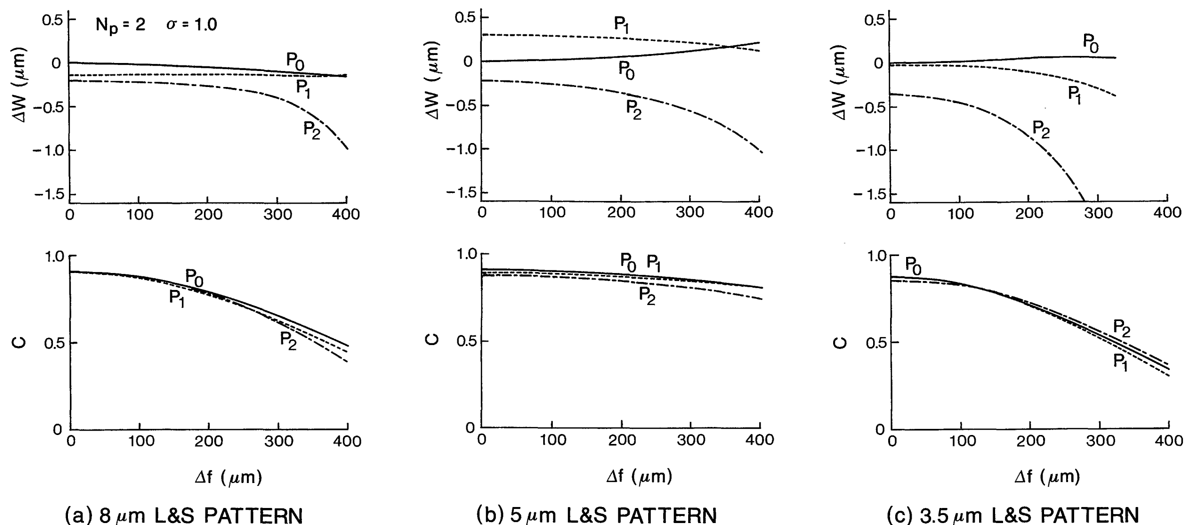

Fig. 13. Effect of Δf on ΔW and C for the 2-points source system with $r_s=0$ and $\sigma=1$. Imaged patterns are (a) 8 μm, (b) 5 μm, and (c) 3.5 μm line-and-space patterns.

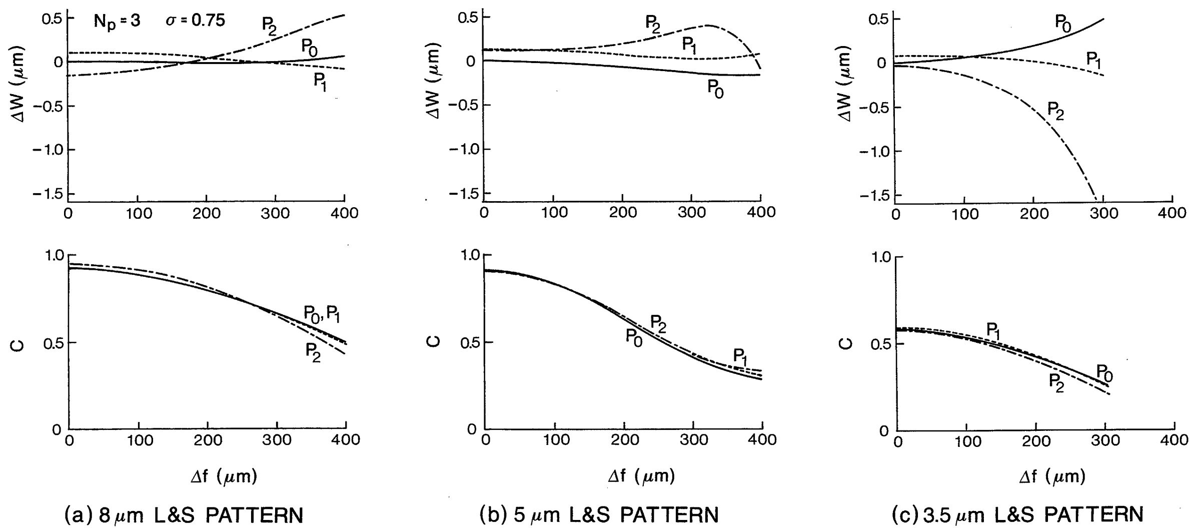

Fig. 15. Effect of Δf on ΔW and C for the 3-points source system with $r_s=0$ and $\sigma=0.75$. Imaged patterns are (a) 8 μm, (b) 5 μm, and (c) 3.5 μm line-and-space patterns.

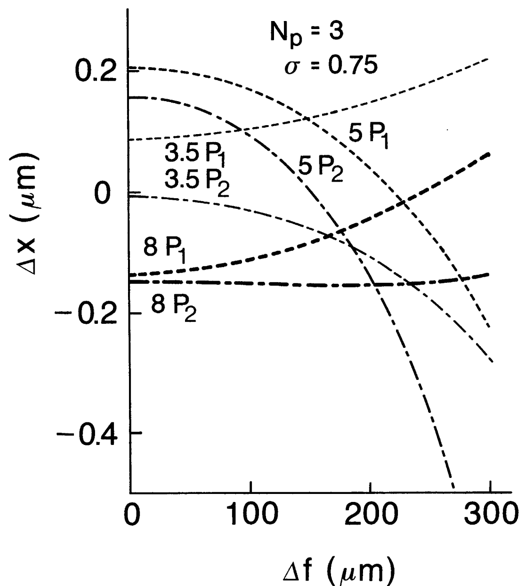

Fig. 16. Relationship between Δf and Δx for P_1 and P_2. The system has a 3-points source with $r_s=0$ and $\sigma=0.75$. Imaged patterns are 8 μm, 5 μm, and 3.5 μm line-and-space patterns.

point sources is 12 for coherence factor $\sigma=1$, and the number varies linearly with σ.

The 2-points source system with $\sigma=1$ produces the most conspicuous focal tolerance characteristics. Especially notable is the focal tolerance for contrast which is about 3 times as large as the system with a plane light source. This effectively improves the resolution. When the 3-points source system with $\sigma=0.75$ is used, intensity distributions with more precise linewidths are obtained while the focal tolerance is maintained almost equal to that due to the plane source system.

In the development of optical projection systems for semiconductor device fabrication, improved resolution has been achieved by developing higher NA projection lenses. An increase in NA narrows the focal tolerance. The analysis shows that it is possible to make the focal tolerance larger and the resolution higher by employing the points source.

Acknowledgments

The author would like to thank Akira Yoshikawa, Yoshiharu Ozaki, and Yoshio Kawai for their valuable advice in discussions.

1) H. H. Hopkins: J. Opt. Soc. Am. **47** (1957) 508.
2) B. J. Lin: IEEE Trans. Electron Devices **ED-27** (1980) 931.
3) R. Barakat: J. Opt. Soc. Am. **52** (1962) 264.
4) T. Asakura and T. Araki: Optik **46** (1976) 365.
5) R. Barakat: J. Opt. Soc. Am. **52** (1962) 276.
6) T. Asakura: Oyo Buturi **31** (1962) 709 [in Japanese].
7) J. W. Goodmann: *Statistical Optics* (John Wiley & Sons, New York, 1985).
8) M. Born and E. Wolf: *Principles of Optics* (Pergamon Press, Oxford, 1980) 6th ed., p. 508.
9) M. D. Levenson, N. S. Viswanathan and R. A. Simpson: IEEE Trans. Electron Devices **ED-29** (1982) 1828.